Tribology - Materials, Surfaces & Interfaces

ISSN: (Print) (Online) Journal homepage: https://www.tandfonline.com/loi/ytrb20

Performance of thermal-sprayed WC-Cr_3C_2-Ni coatings in slurry erosion for hydrodynamic turbines

Digvijay G. Bhosale, Chinmay Dorlikar, Amrut P. Bhosale, Viraj Pasare, Brijesh Maurya, Siddhesh Korgaonkar, Vinay Ginwal & T. Ram Prabhu

To cite this article: Digvijay G. Bhosale, Chinmay Dorlikar, Amrut P. Bhosale, Viraj Pasare, Brijesh Maurya, Siddhesh Korgaonkar, Vinay Ginwal & T. Ram Prabhu (2022) Performance of thermal-sprayed WC-Cr_3C_2-Ni coatings in slurry erosion for hydrodynamic turbines, Tribology - Materials, Surfaces & Interfaces, 16:4, 292-302, DOI: 10.1080/17515831.2022.2078086

To link to this article: https://doi.org/10.1080/17515831.2022.2078086

Published online: 05 Jun 2022.

TRIBOLOGY - MATERIALS, SURFACES & INTERFACES
2022, VOL. 16, NO. 4, 292–302
https://doi.org/10.1080/17515831.2022.2078086

I·M3 Institute of Materials, Minerals & Mining
Taylor & Francis Taylor & Francis Group

RESEARCH ARTICLE

Performance of thermal-sprayed WC-Cr_3C_2-Ni coatings in slurry erosion for hydrodynamic turbines

Digvijay G. Bhosale [a], Chinmay Dorlikar[a], Amrut P. Bhosale[a], Viraj Pasare[b], Brijesh Maurya[a], Siddhesh Korgaonkar[a], Vinay Ginwal[a] and T. Ram Prabhu[c]

[a]Department of Mechanical Engineering, Veermata Jijabai Technological Institute, Mumbai, Maharashtra, India; [b]Department of Mechanical Engineering, D. Y. Patil College of Engineering and Technology, Kolhapur, Maharashtra, India; [c]CEMILAC, Defence Research and Development Organisation, Bangalore, Karnataka, India

ABSTRACT

Hydrodynamic turbine and slurry pump components are frequently influenced by severe wear due to the impact of solid particles present in the water. A WC-based coatings deposited by thermal spray techniques is known for the protection against slurry erosion. In the present work, WC-Cr_3C_2-Ni powder was sprayed on a turbine steel substrate using high-velocity oxy-fuel (HVOF) and atmospheric plasma spray (APS) techniques. Microstructural and phase constitutions of as-sprayed coatings were examined. The effect of speed, slurry concentration and particle size on slurry erosion resistances of both coatings and substrate materials was comparatively studied in a slurry pot erosion tester. The results exhibit that the HVOF coating has better properties in terms of density, micro-hardness and slurry erosion resistance than those of APS coating. The improvement in slurry erosion resistance of bare turbine steel by using APS and HVOF coatings is approximately 37% and 62%, respectively.

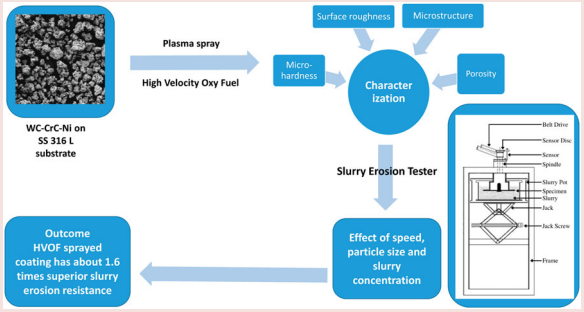

ARTICLE HISTORY
Received 16 December 2021
Accepted 11 May 2022

KEYWORDS
Thermal spray coatings; slurry erosion; turbine steel; tungsten carbide

1. Introduction

One of the challenges faced by hydro-turbine [1] and slurry pump components [2] is slurry erosion, which is usually due to higher momentum solid particles entrained by the liquid, mostly water [1]. The slurry erosion problem becomes especially serious in India during the monsoon season. The solid particle concentration in the water rapidly rises, and therefore, there is a significant increase in the material loss [3,4]. The design life of the hydro-power plant components working in such environments is considerably reduced. Moreover, sometimes failures of components lead to unavoidable close-down of power plant operations. The main constituent of solid particles in the slurry in this application is micro quartz (SiO_2), which is responsible for severe erosion [4–7]. The estimated financial loss due to slurry erosion in India is 120–150 million USD [8]. Consequently, slurry erosion in hydro-power plants needs to be minimised for better efficiency and lower operational and maintenance costs. In recent years, a CF8M turbine steel is mostly used as an alloy, which possesses good mechanical properties, but it has poor slurry erosion resistance. The severe slurry erosion degrades this steel speedily because the hardness of the steel is considerably lower compared to the hardness of solid particles. Therefore, the usage of surface engineering techniques, particularly thermal spray coatings is helpful for improvement in the hardness and slurry erosion resistance of turbine steel [4]. The tungsten carbide and/or chromium carbide hard metal coatings could be an ideal choice as a protective coating against slurry erosion [9].

Every thermal spray process has its unique characteristics, but available literature recommends that high-velocity oxy-fuel and plasma spray processes provide capable solutions to combat erosion [4,9–13]. The material removal by slurry erosion in thermal-sprayed coatings depends on impingement

CONTACT Digvijay G. Bhosale digvijay_bhonsale@yahoo.co.in

conditions [10,14–16], solid particle properties [9,10,14,17], target material properties [18] and slurry characteristics [10,17]. The hardness of the target surface, velocity, particle size and slurry concentration are responsible for the increase in the stresses induced on the coating [9–17], and therefore, investigating the effect of these parameters on the coating is a vital aspect for a comprehensive understanding of slurry erosion mechanisms. The prediction of the slurry erosion mechanism is a complicated phenomenon due to the interaction parameters mentioned above. Generally, deformation and micro-cutting are two preliminary processes that are accountable for erosion [4]. A plastic deformation [13,19], penetration of cutting edge [13,19–21], cyclic fatigue [20], brittle fracture [9,22], material removal at weak splat interface [9,14], micro-cracks initiation [10,11,17], micro-ploughing [10,19,20], craters and pits [10,11,16,17], eruption on binder [11,17], extrusion of soft metal matrix [16,21,22] are reported material removal mechanisms by erosion in thermal spray coatings. At lower impact angles, micro-cutting is the leading mechanism. However, the initiation of sub-surface cracks and deformation mechanisms is detected when solid particles are impacted on the surface at a normal angle with significant energy.

Tungsten carbide-based coatings are mostly preferred in aggressive environments to increase wear resistance and improve erosion resistance [11–14,23–29]. Further, the corrosion resistance of WC-based coating increases with the addition of chromium to the matrix [22,30]. The dispersion of WC in a metal matrix of WC-Cr_3C_2-Ni coating provides high erosion resistance and high hardness [12,26,31], and Cr helps to enhance corrosion resistance [22,23,26,32]. Therefore, WC-Cr_3C_2-Ni coating is an appropriate choice for the components working underwater where the erosion-corrosion phenomenon is dominant. Moreover, the literature shows that few information is available on the slurry erosion behaviour of high-velocity oxy-fuel and atmospheric plasma-sprayed WC-Cr_3C_2-Ni coatings, and the effect of slurry concentration, particle size and velocity on WC-Cr_3C_2-Ni coating.

Therefore, the present study aims to investigate the applicability of WC-Cr_3C_2-Ni coating on hydrodynamic turbines and slurry pump components. A deposited coating and uncoated turbine steel are tested in a slurry pot erosion tester to study the effect of slurry concentration, velocity and particle size on slurry erosion behaviour. The phase composition, surface and cross-section characteristics, mechanical properties and slurry erosion resistance of both coatings were extensively analysed. Further, slurry erosion mechanisms are explored and discussed. The study provides useful information about the behaviour of thermal-sprayed WC-Cr_3C_2-Ni coatings in slurry erosive environments.

2. Experimental procedures

2.1. Materials and coatings preparation

The ASTM A743 steel was selected as a substrate material because of its extensive use in hydrodynamic turbine components. Table 1 presents the chemical composition of ASTM A743 steel.

Two thermal spray techniques namely, HVOF and APS were used to deposit commercially available WC-Cr_3C_2-Ni powder on ASTM A743 steel. The mean particle size of feedstock powder was 37 µm, and the manufacturer was H. C. Starck, Germany. The powder was produced by an agglomerated and sintered process, which was composed of nickel 7.3%, chromium carbide 19.7%, balanced by tungsten carbide. Before the coating deposition process, the ASTM A743 steel substrate was grit blasted using blasting parameters given in Table 2. The APS and HVOF coating deposition is carried out at MECPL, Jodhpur, India, using MF-4MB and Hipojet 2700 torch, respectively, with the deposition parameters listed in Table 2. The torches are manufactured by MECPL, Jodhpur, India. Before deposition, substrate preheating is carried out to reduce the degree of distortion. The substrate preheating is not a sufficient solution, and therefore, adding a buffer layer (having an intermediate coefficient of thermal expansion) between the coating and the substrate is recommended [33,34]. Although, the slurry erosion resistance of the topmost surface of coatings is unaffected, which is the primary aim of current research.

2.2. Characterisation

The X-ray diffraction with Cu-Kα radiation (XRD, Malvern Panalytical) was used for the identification

Table 2. APS and HVOF process parameters.

Process parameters	APS	HVOF
Blasting pressure (Bar)	5	5
Blasting distance (mm)	150	150
Blasting angle (°)	90	90
Standoff distance (mm)	127	150
Particle velocity (m/s)	131	534
Powder feed rate (g/min)	40	45
Gun traverse speed (m/s)	0.7	0.7
Plasma arc current (A)	500	–
Ar gas flow rate (SLPM)	40	–
H_2 gas flow rate (SLPM)	4	–
Oxygen flow rate (SLPM)	–	240
Propane flow rate (SLPM)	–	60

Table 1. Chemical Composition for the ASTM A743 (%weight).

Grade	C	Mn	Si	*P*	S	Cr	Mo	Ni	Fe
ASTM A743	0.03	1.5	1.5	0.045	0.03	19.0	2.0	10.0	Balance

of phases in the powder and as-deposited coatings. A surface and cross-section morphologies of as-deposited coatings and slurry-eroded surfaces were studied by field emission scanning electron microscope with EDS attachment (ZEISS Gemini). The image analysis method (ImageJ software) was used for porosity measurement on the polished cross-section of the coatings. The ideal parameters for porosity measurement using the image analysis technique were roughness of 0.1 µm, fields of view 15 and magnification 1000× [35], which was used in the measurement of porosity percentage. The micro-hardness of both coatings and steel was measured using a Vickers microhardness tester (CSM Instruments, Switzerland). The hardness was measured on polished specimens across the coating thickness with holding time of 15 s at a maximum load of 2.942 N. The surface roughness tester (Mitutoyo SJ 210) was utilised for surface roughness measurement of as-deposited coatings.

2.3. Slurry erosion test

The slurry pot erosion tester capable of holding six samples was used to study the slurry erosive behaviour of both uncoated and coated specimens. The maximum speed of the setup was 3000 rpm. Six spindles were provided for the purpose of fitting specimens with the help of a screw. A separate stainless steel slurry pot was provided for every specimen. The specimens were dipped in the pot, which was filled with a slurry of water and 100 and 300 µm alumina (Al_2O_3). The walls of the slurry pot contain four vertical baffles, which promote turbulence in the slurry. The fresh slurry was prepared before every test. Only one surface of both coated and uncoated specimens was exposed to the slurry, and other surfaces were masked. This provision helped to avoid slurry erosion of undesirable surfaces of every specimen. The investigation was carried out at two erodent concentrations by weight of 10% and 20% under two-speed conditions (1000 and 3000 rpm). Every test was repeated three times for a maximum test duration of 7 h. Figure 1 presents a schematic presentation of the slurry erosion tester used in this investigation.

Before and after the slurry erosion test, the specimens were ultrasonically cleaned, dried and weighted with a weight balance having a precision of 0.1 mg. The cleaning process ensures the removal of any loosely bonded dirt, debris or erodent particles from the surfaces of the specimens.

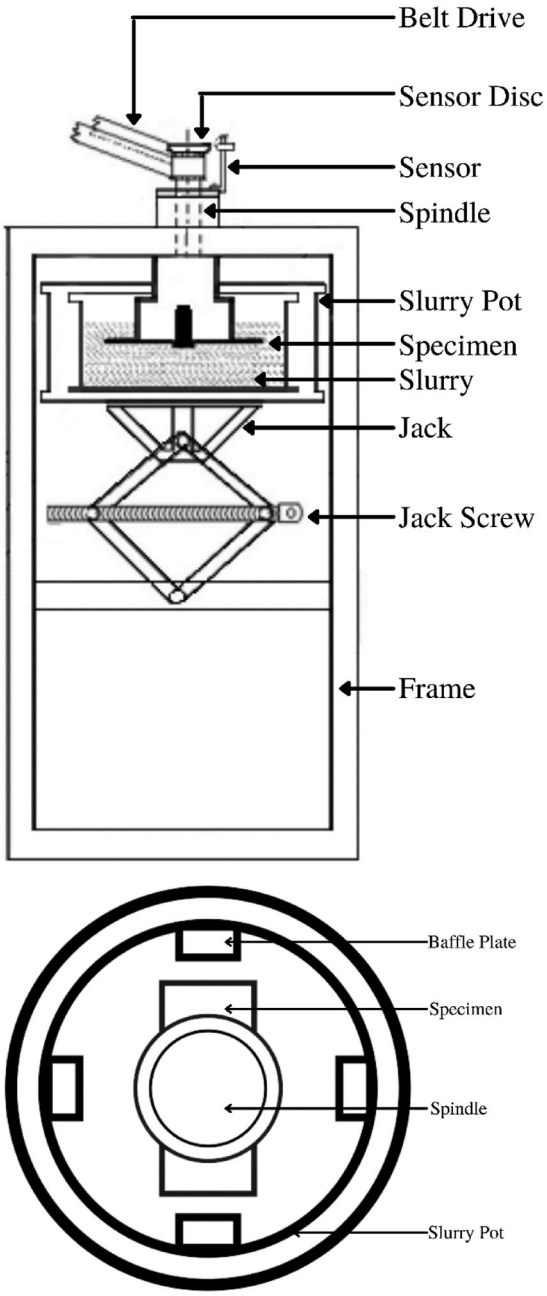

Figure 1. Schematic diagram of slurry erosion tester used in the investigation.

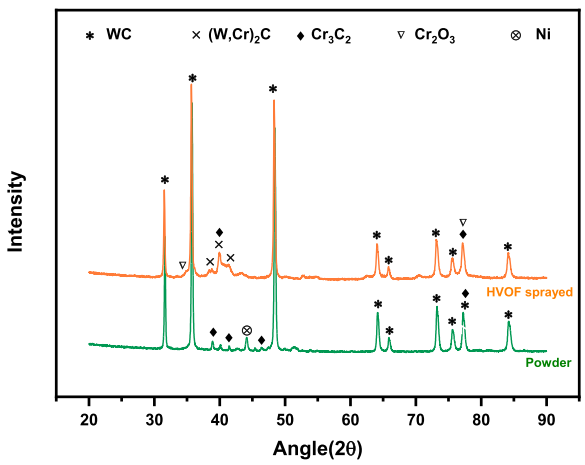

Figure 2. XRD analysis of as-received feedstock powder and HVOF as-sprayed WC-Cr_3C_2-Ni coating.

3. Results and discussion

3.1. Compositional analysis

Figure 2 shows the compositional analysis of as-received powder and as-deposited HVOF coating.

The main constituent in the powder is WC along with a binder alloyed Ni. A chromium carbide peaks are somewhat shifted as compared with standard X-ray diffraction patterns. The phase $(W,Cr)_2C$ is absent in the powder, which is identified in the powder produced by other manufacturers [36].

During the deposition of coating by the HVOF technique, phase $(W,Cr)_2C$ is developed. The peaks of $(W,Cr)_2C$ are less intense and broader than the peaks of the WC phase. The metallic Ni is present in a small amount in the feedstock powder. Therefore, peaks of Ni are not detected in the as-deposited HVOF coating. Traces of chromium oxide are identified in the HVOF coating.

A diffraction pattern of as-deposited coating by APS is shown in Figure 3. The phase $(W,Cr)_2C$ has a significantly more intense peak in APS coating than that of HVOF coating. The W_2C has higher brittleness than the WC phase, and therefore, the presence of a greater degree of W_2C in as-sprayed coating degrades the coatings due to erosion. The WC has a hardness of 24 GPa, which is much lesser than the hardness of W_2C (30 GPa). Moreover, fracture toughness and elastic modulus of W_2C are lower than the WC phase [37–40]. The rapid cooling and high process temperature cause the appearance of WC_{1-x} in the APS coating, as confirmed by the XRD analysis. Consequently, different cooling rates involved in the HVOF and APS processes govern compositional changes in the as-sprayed coatings. The phase volume of Ni is less than the detection limit of the diffractometer, and therefore, Ni is not identified in the APS coating.

3.2. Microstructure and porosity

The initial cross-sectional microstructure of HVOF and APS coatings is presented in Figure 4. The average coating thickness of both as-deposited coatings is measured using ImageJ software and presented in Figure 4(a,c). The HVOF coating has a comparatively dense structure. Moreover, both coatings consist of a defect-free substrate and coating interface without delamination. A typical characteristic of any thermal spray coating is laminar splat alike microstructure, which is visible in the cross-section of both coatings (refer Figure 4(c,d)).

The EDS analysis on a cross-section of both coatings is presented in Table 3, which is used in combination with SEM for mapping the elemental composition. The analysis suggests that the cross-sectional microstructure consists of decarburised WC and chromium carbide (refer to A1–A3 and B1–B3 points in Figure 4(b,d) and respective analyses in Table 3), and their stoichiometric composition is analogous to decarburised W_2C and chromium carbide $Cr_{23}C_6$. The W_2C is formed in both coatings but not detected by the X-ray diffractometer probably because the W_2C phase volume concentration is less than the detection limit.

Figure 5(a,b) presents interlocked splats in the surface microstructure of as-sprayed HVOF and APS coatings, respectively. Partially melted powder particles are embedded in the fully melted splats, which are detected at a few locations. This feature is more in the HVOF coating because of the lower processing temperature.

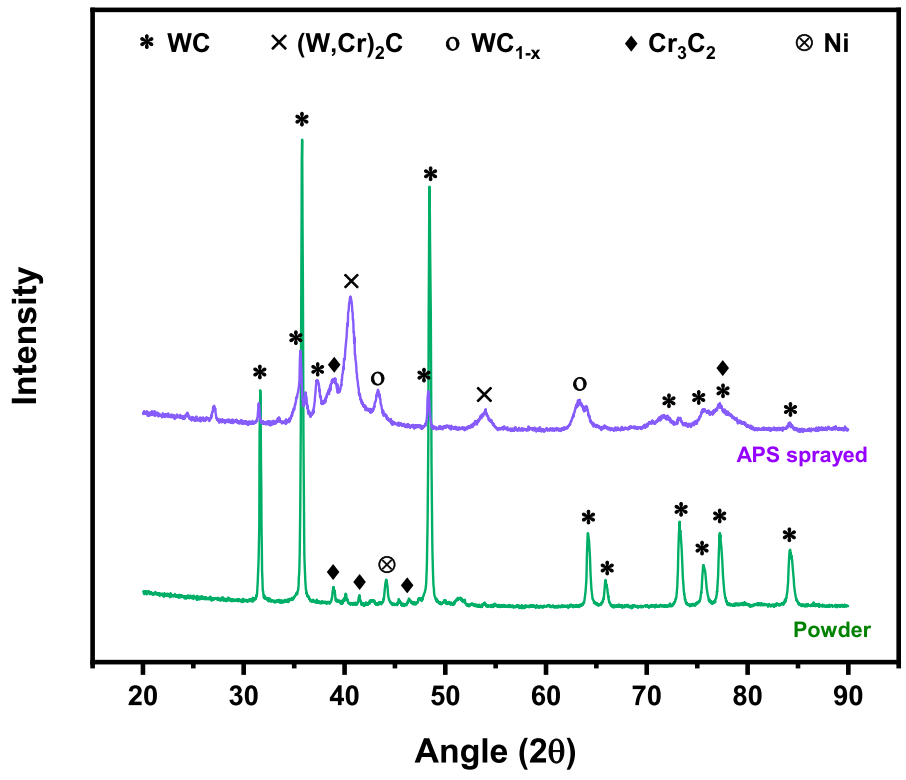

Figure 3. XRD analysis of as-received feedstock powder and APS as-sprayed WC-Cr_3C_2-Ni coating.

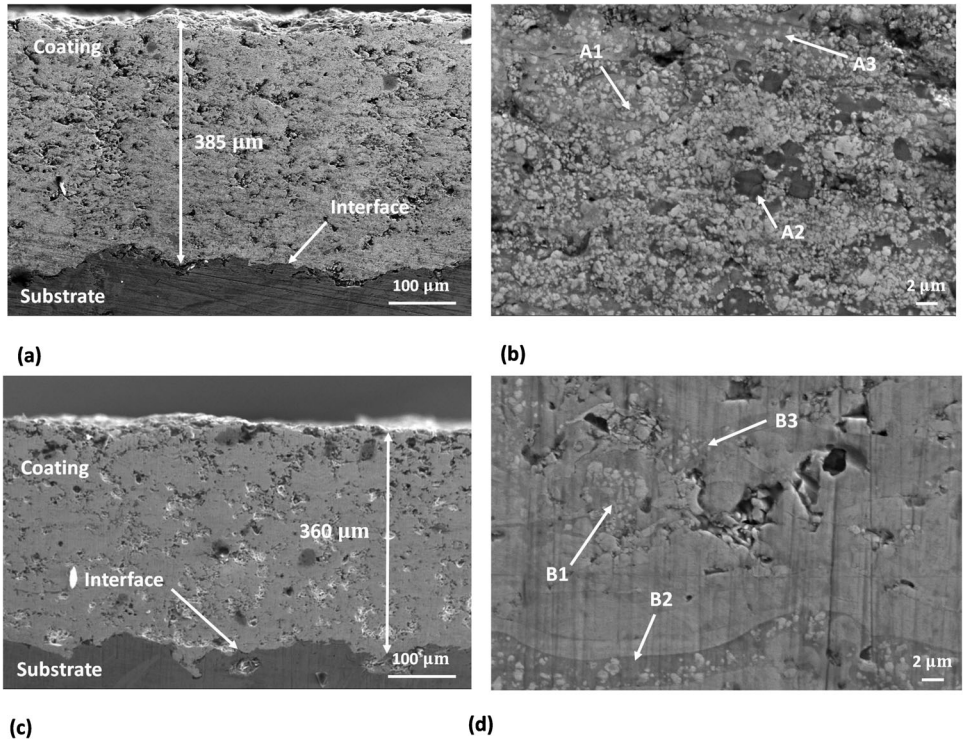

Figure 4. Cross-sectional microstructures of as-sprayed (a, b) HVOF and (c, d) APS coatings at low (400×) and high magnifications (5000×).

Table 3. EDS analysis of HVOF and APS coatings.

Coatings	Points in Figure 3	Elements in % at. W	C	Cr	Ni	O
HVOF	A1	60.2	13.1	16.2	6.0	4.5
	A2	2.7	16.5	69.3	5.7	5.8
	A3	65.1	12.5	13.4	4.2	4.9
APS	B1	63.4	14.2	14.3	4.7	3.5
	B2	14.7	20.1	54.2	6.1	4.9
	B3	61.3	11.0	14.5	3.7	9.5

The SEM micrographs of both coatings exhibit the existence of a few micro-voids on the surfaces, which is an integral feature of thermal spray coatings.

The presence of pores in the HVOF, 0.5 ± 0.2%, is lower than that in the APS coating, which is 1.6 ± 0.3%. The values are consistent with the porosity percentage reported in the literature on HVOF and APS-deposited WC-based coatings. The porosity content in HVOF-sprayed WC-Cr_3C_2-Ni appears lower compared to WC-10Co-4Cr coatings [9,21,41]. The reduction in the porosity is because of the lower melting point of WC-Cr_3C_2-Ni (1250°C), compared to 1480°C for WC-10Co-4Cr [42,43]. This is probably due to an increase in the percentage share of Cr_3C_2 in the composition. The condition to escape gases from the molten material is more favourable in the case of WC-Cr_3C_2-Ni coating since there is an increase in the duration of the liquid state of the molten material. The presence of porosity underneath the surface reduces the erosion resistance of the coatings.

3.3. Micro-hardness

The slurry erosion resistance of the coatings is correlated to the hardness. Figure 6 presents micro-hardness variation for both HVOF and APS coatings. The HVOF-processed coating shows higher hardness

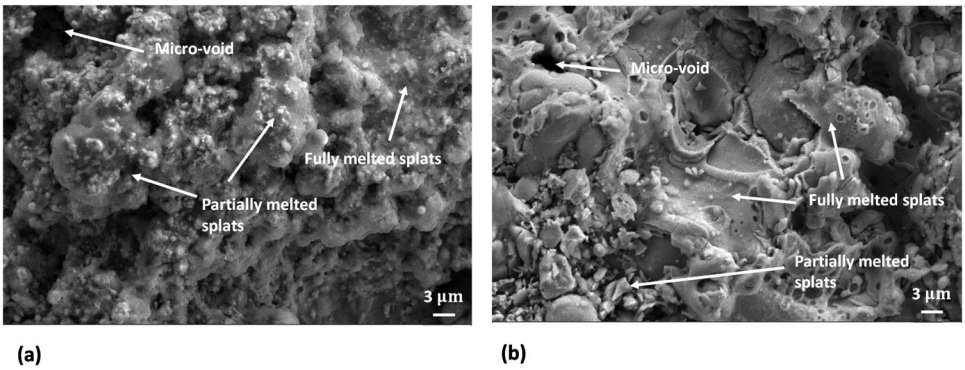

Figure 5. Surface microstructures of as-sprayed (a) HVOF and (b) APS coatings.

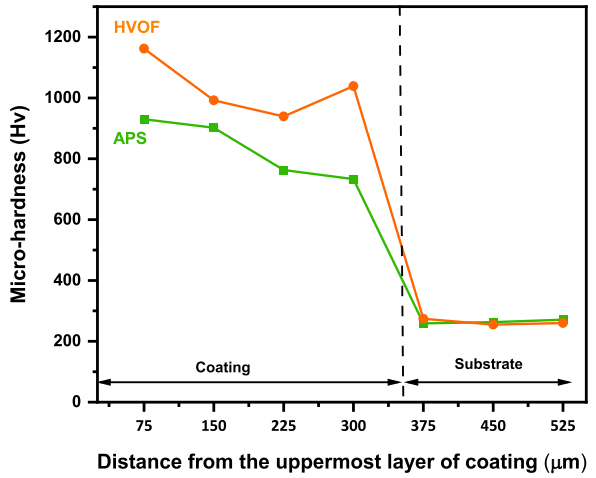

Figure 6. Variation micro-hardness of HVOF and APS coatings from coated surface to substrate.

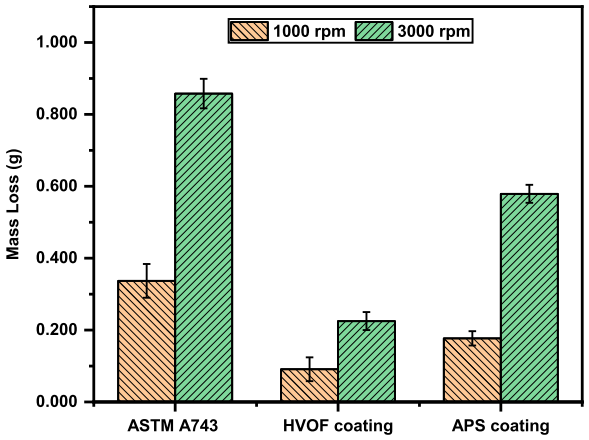

Figure 7. Variation of mass loss of coated and uncoated specimens with change in speed of rotation.

than that of the APS-processed coating. The maximum hardness is measured near the uppermost layer of the coating surfaces, which is 1162 and 930 HV for HVOF and APS coatings, respectively. A splat adhesion and degree of porosity in the as-sprayed coatings affect the micro-hardness. The HVOF coating has a lower porosity level and comparatively good splat adhesion, and therefore, resulted in higher micro-hardness. The higher hardness of the HVOF coating is attributed to the higher percentage of hard WC phase in the coating composition. The matrix $(W,Cr)_2C$ detected in the APS coating is less hard as compared to the WC phase. Moreover, a decrease in the micro-hardness across the coating cross-section of APS coating is observed, and it is minimum near the bottom layer of coating. Interestingly, an increase in the hardness of the HVOF coating near the bottom layer is observed. This is because higher compressive residual stresses contributed to the HVOF coating formation. The results show that the hardness of the ASTM A743 steel substrate could be increased by five and four times using HVOF and APS-sprayed WC-Cr_3C_2-Ni coatings, respectively.

3.4. Slurry erosion performance

As described earlier, the performance of both coatings and uncoated steel against slurry erosion is tested, and the effect of speed, slurry concentration and particle size on slurry erosion resistance is comparatively investigated.

3.4.1. Effect of speed

The mass loss of uncoated and coated specimens with variation in the speed of rotation is presented in Figure 7. All results presented are for 7 h test duration with erodent particle size 300 μm and 20% slurry concentration by weight. The maximum erosion is recorded at 3000 rpm for coated and uncoated specimens. An increase in speed of rotation resulted in an increase in the mass loss of coated and uncoated specimens. This is expected since an increase in speed also increases the kinetic energy and momentum of erodent particles present in the slurry. The hard erodent particles with the amplified momentum will be responsible for the local attacks on several locations on the coating surface, which results in plastic deformation and micro-cracking. These mechanisms help excessive material removal from the surface of coated specimens. However, APS coating exhibits approximately three times more material loss as compared to HVOF coating due to the availability of more weak spots in the form of decarburised WC and porosity. Therefore, the material removal rate by slurry erosion is directly proportional to the speed of rotation. The results are in good agreement with the results presented by another researcher [44]. The results show that the effect of speed is maximum on the uncoated specimens and almost the same on both coated specimens. Since the slurry erosion rate is generally directly proportional to the momentum of erodent particles, slurry erosion resistance is enhanced by 41% in the case of APS coatings. Moreover, usage of HVOF coating increases slurry erosion resistance by three times than uncoated steel.

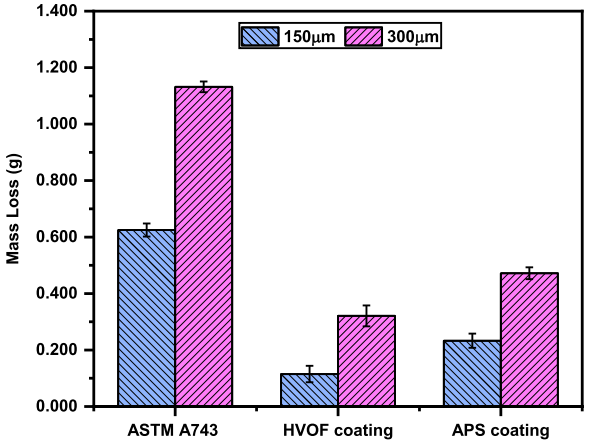

Figure 8. Variation of mass loss of coated and uncoated specimens with increase in speed of rotation.

3.4.2. Effect of particle size

Figure 8 presents the mass loss of uncoated and coated specimens with variations in the particle size. The test duration for every experiment was 7 h. Tests were conducted at 3000 rpm and 20% slurry concentration by weight. The momentum and kinetic energy of large-sized erodent particles are more, and therefore they are capable of localised material removal from the target surface even with few interactions. However, small-sized erodent particles have comparatively lower impact force, and they are also subjected to retardation before impacting the target surface. Therefore, the collision effectiveness of small-sized particles is lower than that of large-sized particles, which caused a lower transfer of energy during the impact. Thus, the erosion rate of both coatings and uncoated specimens increases with an increase in the particle size of the erodent. Moreover, the marginal mass loss is reported for both coatings when compared with uncoated specimens, even in the presence of large-sized particles. A significant increase in the hardness of coated specimens is contributed to the reduction in the localised material removal. The outcomes show that the change in particle size has more effect on HVOF coating rather than APS coating. The results here are in agreement with other researchers [45–47]. The change in particle size increases the material loss of coatings by 300% and 250% for HVOF and APS coatings, respectively.

3.4.3. Effect of slurry concentration

Figure 9 shows the mass loss of uncoated and coated specimens due to slurry with variation in the concentration. The testing parameters duration, particle size and speed are 7 h, 300 μm and 3000 rpm, respectively. The results show that with an increase in slurry concentration by weight from 10% to 20%, the erosion also increases for all specimens under the study. The target surfaces of specimens are exposed to more impingements of erodent particles when slurry concentration changes from 10% to 20%. The mass loss of uncoated and APS-coated specimens increases significantly with the increase in the slurry concentration. However, there is a marginal increase in the mass loss of HVOF coating due to an increase in concentration. The HVOF-coated specimen has reduced the mass loss of ASTM A743 steel by approximately 76% and 84% in the presence of a slurry of 10% and 20% concentrations. Moreover, APS coating is also useful to enhance the slurry erosion resistance of ASTM A743 steel by approximately 1.7 times. A significant difference in the hardness of ASTM A743 steel and Al_2O_3 erodent particles is attributed to the larger material removal for steel as compared to both coatings.

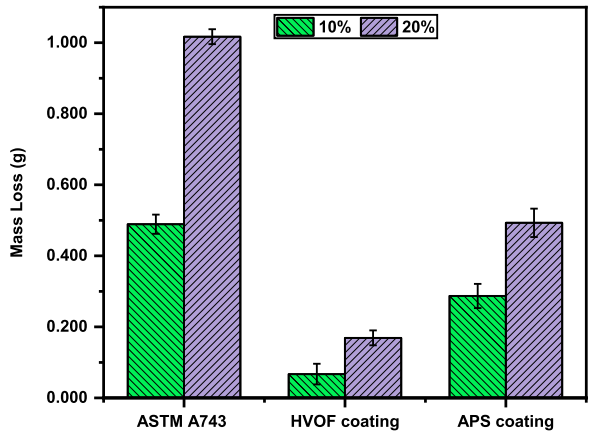

Figure 9. Effect of slurry concentration on erosion performance of coated and uncoated specimens.

3.5. Eroded surface morphology

The erodent impingement angle and properties of the material are the major factors affecting the slurry erosion mechanisms. The principal erosion mechanisms in hydrodynamic components are ductile deformation, brittle fracture and surface fatigue [48]. However, micro-cutting and repetitive plastic deformation are two mechanisms that affect material removal rate by erosion. The erodent impingement angle has a great influence on the erosion mechanism. The micro-cutting and chip formation are dominant at lower impingement of erodent. However, with an increase in the impingement angle near to normal to the surface, the intensity of lips and craters increases, which subsequently forms plate-like debris [49]. The eroded surfaces of hydrodynamic components exhibit signs of both types of mechanisms since the silt entrained in the water impinges on the surface at any impingement angle.

3.5.1. HVOF coating

The defects in the coating act as weak zones. Therefore, the excessive material removal from coating surfaces initiates mostly through the removal of the soft matrix binder and defects. The eroded surfaces of HVOF coating for two different operating conditions are presented in Figure 10. The impact of high momentum erodent particles has contributed to the removal of micro-hills and loosely bounded grains from the coating surface. Therefore, the comparison of the eroded surface with the as-deposited HVOF coating surface (Figure 5) demonstrates that the eroded surface is relatively smoother. The un-melted particles due to lower particle temperature and degree of melting are inherent characteristics of the HVOF coating. Figure 10(a) presents un-melted particles detached locations, which are removed from the coating surface because of their low bonding. The plastic deformation or ploughing results in micro-cutting marks that are visible on the eroded surfaces in Figure

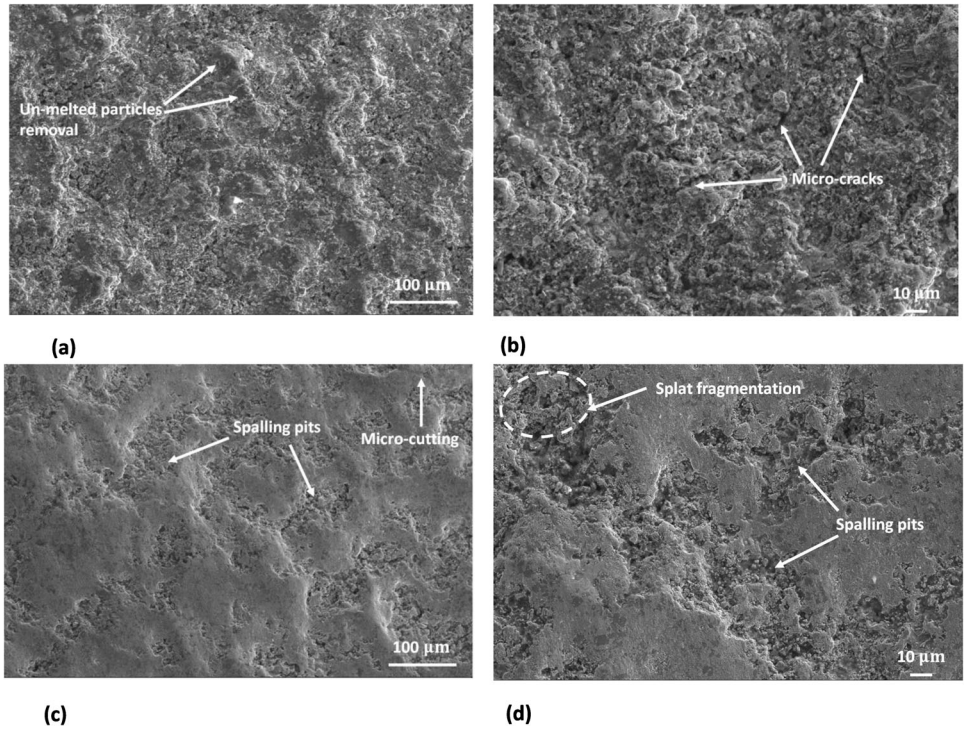

Figure 10. SEM micrographs of slurry-eroded surfaces of HVOF coating (a, b) 1000 rpm, 100 µm particle size and 10% slurry concentration by weight and (c, d) 3000 rpm, 300 µm particle size and 20% slurry concentration by weight.

10(b,c). The splat fragmentation is a consequence of the removed binder phase that destabilises carbide grains, and the subsequent impacts of erodent further take away carbide grains leaving behind spalling pits, as shown in Figure 10(c,d). Similar observations were reported by other researchers [50,51]. Further, the debonding of splats is the noticeable feature for the HVOF coating tested at higher speed, larger erodent particle size and more slurry concentration (Figure 10(c,d)), which is absent when these operating parameters are lower (Figure 10(a,b)).

3.5.2. APS coating

In Figure 11, the wear mechanisms reported for APS coating are craters, carbide pull out, splat fragmentation and delamination. Significant erosive wear is

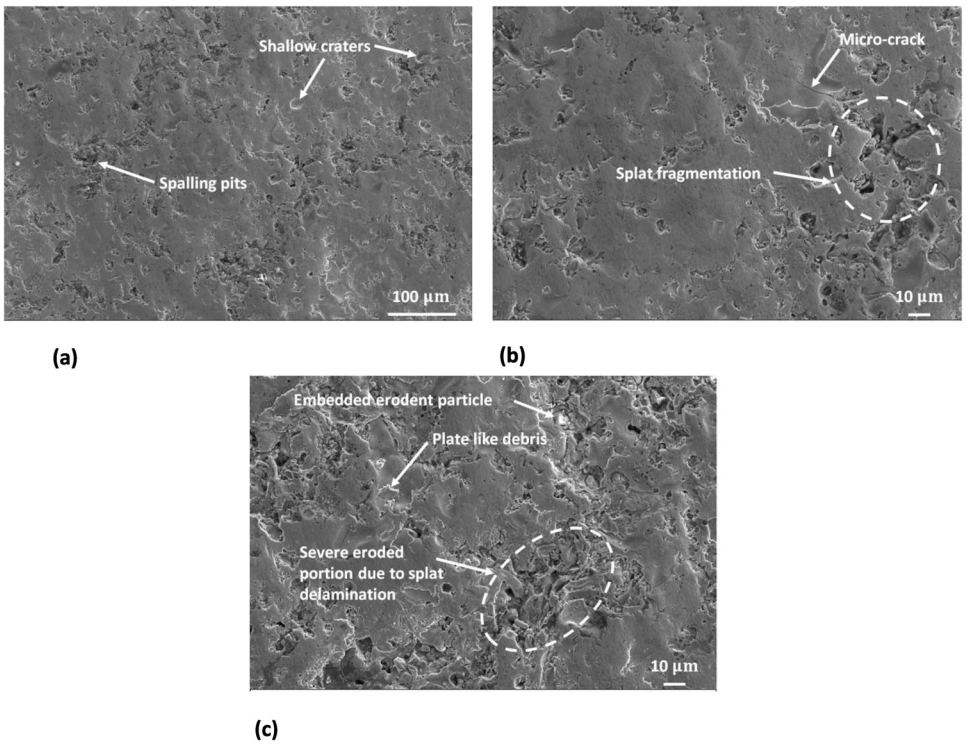

Figure 11. SEM micrographs of slurry-eroded surfaces of APS coating (a, b) 1000 rpm, 100 µm particle size and 10% slurry concentration by weight and (c) 3000 rpm, 300 µm particle size and 20% slurry concentration by weight.

noticed on the surfaces of APS coating. A shallow crater developed due to the normal impact of erodent is marked in Figure 11(a). A high-energy repetitive impacts of erodent are responsible for micro-crack nucleation (refer to Figure 11(b)), and over the period, cracks propagate on the coating surface. The micro-crack combines with the deformation to cause splat delamination and soft binder eruption. With an increase in the impingement angle near to normal to the surface at a higher speed, the intensity of lips and craters increases, which subsequently forms plate-like debris presented in Figure 11(c). The severely eroded regions because of localised material removal are observed throughout tested APS specimens, which imply that the slurry erosion resistance of APS coating is comparatively lower than that of the HVOF coating.

The kinetic energy associated with a single erodent particle increases by a magnitude of three orders when the particle diameter is increased by a magnitude of one order. The large-sized particles would not simply follow the flow of slurry, and consequently, particle impingement angle tends to increase. The defects in the coating have a lesser contribution to overall material removal whenever the impingement angle and kinetic energy of erodent increase. Therefore, eroded surfaces of both coatings at 3000 rpm show spalling pits due to the loss of extruded material by successive impacts of erodent particles.

The material removal in the form of spalling pits on both coating surfaces is localised wear that occurs near the coating defects such as decarburised phase W_2C, porosity. This fact highlights the necessity of a homogeneous coating structure with a smaller number of weak regions. The improved cohesion and more homogeneous coating structure are possible with the lower porosity, high modulus of elasticity and negligible deviation in the micro-hardness values. Indeed, HVOF coating has lesser porosity and higher micro-hardness as compared to the APS coating. Therefore, the HVOF coating exhibited superior resistance to slurry than the APS coating.

4. Conclusions

The investigation was focused on the slurry erosion behaviour of APS and HVOF-deposited WC-Cr_3C_2-Ni coatings with variation in speed, erodent particle size and slurry concentration. The results will serve as initial data needed during the selection of coatings for hydrodynamic turbines and slurry pumps components. The useful outcomes are as follows:

1. The variations in phase composition and microstructure are observed in as-sprayed HVOF and APS coatings. The APS coating contains a significant amount of brittle (W, Cr)$_2$C phase due to extensive interaction between the carbides. The relatively dense morphological structure and higher hardness of HVOF-sprayed WC-Cr_3C_2-Ni coating are observed. The per cent of pores ($0.5 \pm 0.2\%$) in the HVOF coating is lower than that in the APS coating ($1.6 \pm 0.3\%$). Compact and defect-free coating-substrate interface, dense morphological structure and higher average hardness are prerequisites for enhancing the slurry erosion resistance of HVOF coatings.
2. The HVOF-sprayed coating has about 1.6 times superior slurry erosion resistance over APS-sprayed coatings. A lesser porosity and higher micro-hardness, in the HVOF coating, are favourable aspects in building up a more homogeneous coating structure and improvement in the cohesion.
3. The speed of rotation is a dominant factor for an increase in the material removal rate of all investigated specimens. The effect of speed is maximum on the uncoated specimens and almost the same on both coated specimens.
4. The change in particle size increases the material loss of coatings by 300% and 250% for HVOF and APS coatings, respectively.
5. Both coatings are equally affected by the change in the slurry concentration. The HVOF-coated specimen has reduced the mass loss of ASTM A743 steel by approximately 76% and 84%, respectively, in the presence of a slurry of 10% and 20% concentrations by weight.

Acknowledgements

The authors wish to thank Metallizing Equipment Pvt. Ltd., Jodhpur, India, for providing the coating facility. The authors are grateful to IIT Bombay, India, for providing the testing facilities such as SEM, EDX, XRD and micro-indentation. This research work did not receive any specific grant from funding agencies in the public, commercial or not-for-profit sectors.

Disclosure statement

No potential conflict of interest was reported by the author(s).

ORCID

Digvijay G. Bhosale http://orcid.org/0000-0002-0432-6791

References

[1] Wood RJK, Jones TF, Ganeshalingam J, et al. Comparison of predicted and experimented erosion estimates in slurry ducts. Wear. 2004;256:937–947.
[2] Llewellyn RJ, Yick SK, Dolman KF. Scouring erosion resistance of metallic materials used in slurry pump service. Wear. 2004;256:592–599.

[3] Naidu BSK. Developing silt consciousness in the minds of hydropower engineers. Proceedings of the 1st International Conference on Silting Problems in Hydropower Plants; 1999. p. 1–36.
[4] Prashar G, Vasudev H, Thakur L. Performance of different coating materials against slurry erosion failure in hydrodynamic turbines: a review. Eng Fail Anal. 2020;115:104622.
[5] Zu JB, Hutchings IM, Burstein GT. Design of a slurry erosion test rig. Wear. 1990;140:331–344.
[6] Feng Z, Ball A. The erosion of four materials using seven erodents – towards an understanding. Wear. 1999;233–235:674–684.
[7] Ludwiga GA, Malfatti CF, Schroedera RM, et al. Performance of different coating materials against slurry erosion failure in hydrodynamic turbines: a review. Surf Coat Technol. 2019;377:124918.
[8] Mann BS, Arya V. Abrasive and erosive wear characteristics of plasma nitriding and HVOF coatings: their application in hydro turbines. Wear. 2001;249:354–360.
[9] Matikainen V, Rubio Peregrina S, Ojala N, et al. Erosion wear performance of WC-10Co_4Cr and Cr_3C_2-25NiCr coatings sprayed with high-velocity thermal spray processes. Surf Coat Technol. 2019;377:196–212.
[10] Ramesh CS, Devaraj DS, Keshavamurthy R, et al. Slurry erosive wear behaviour of thermally sprayed Inconel-718 coatings by APS process. Wear. 2011;271:1365–1371.
[11] Thakur L, Arora N. A comparative study on slurry and dry erosion behaviour of HVOF sprayed WC–CoCr coatings. Wear. 2013;303:405–411.
[12] Bhosale DG, Prabhu TR, Rathod WS. Sliding and erosion wear behaviour of thermal sprayed WC-Cr_3C_2-Ni coatings. Surf Coat Technol. 2020;400:126192.
[13] Wang Q, Tang Z, Cha L. Cavitation and sand slurry erosion resistances of WC-10Co-4Cr coatings. J Mater Eng Perform. 2015;24:2435–2443.
[14] Bansal A, Singh J, Singh H. Slurry erosion behavior of HVOF-sprayed WC-10Co-4Cr coated SS 316 steel with and without PTFE modification. J Therm Spray Technol. 2019;28:1448–1465.
[15] Grewal HS, Singh H, Arora HS, et al. Zirconium based bulk metallic glass – better resistance to slurry erosion compared to hydroturbine steel. Wear. 2013;307:28–34.
[16] Arji R, Dwivedi DK, Gupta SR. Some studies on slurry erosion of flame sprayed Ni-Cr-Si-B coating. Ind Lubr Tribol. 2009;61:4–10.
[17] Thakur L, Arora N, Jayaganthan R, et al. An investigation on erosion behavior of HVOF sprayed WC–CoCr coatings. Appl Surf Sci. 2011;258:1225–1234.
[18] Goyal K. Experimental investigations of mechanical properties and slurry erosion behaviour of high velocity oxy fuel and plasma sprayed Cr_2O_3 – 50% Al_2O_3 coatings on CA6NM turbine steel under hydro accelerated conditions. Tribol Mater, Surf Interfaces. 2018;12:97–106.
[19] E M, Hu HX, Guo XM, et al. Comparison of the cavitation erosion and slurry erosion behavior of cobalt based and nickel-based coatings. Wear. 2019;428–429:246–257.
[20] Santa JF, Baena JC, Toro A. Slurry erosion of thermal spray coatings and stainless steels for hydraulic machinery. Wear. 2007;263:258–264.
[21] Yoganandh J, Natarajan S, Kumaresh Babu SP. Erosion behaviour of WC–Co–Cr thermal spray coated grey cast iron under mining environment. Trans Indian Inst Met. 2013;66:437–443.
[22] Liu J, Chen T, Yuan C, et al. Performance analysis of cavitation erosion resistance and corrosion behavior of HVOF-sprayed WC-10Co-4Cr, WC-12Co, and Cr_3C_2-NiCr coatings. J Therm Spray Technol. 2020;29:798–810.
[23] Bhosale DG, Rathod WS. Investigation on wear behaviour of SS 316L, atmospheric plasma and high velocity oxy-fuel sprayed WC-Cr_3C_2-Ni coatings for fracturing tools. Surf Coat Technol. 2020;390:125679.
[24] González MA, Rodríguez E, Mojardín E, et al. Study of the erosive wear behaviour of cryogenically and tempered WC-CoCr coating deposited by HVOF. Wear. 2017;376–377:595–607.
[25] Kumar A, Sharma A, Goel SK. Erosion behaviour of WC-10Co-4Cr coating on 23-8-N nitronic steel by HVOF thermal spraying. Appl Surf Sci. 2016;370:418–426.
[26] Bolelli G, Berger L-M, Bonetti M, et al. Comparative study of the dry sliding wear behaviour of HVOF-sprayed WC–$(W,Cr)_2C$–Ni and WC–CoCr hard metal coatings. Wear. 2014;309:96–111.
[27] Bhosale DG, Rathod WS. Tribo-behaviour of APS and HVOF sprayed WC–Cr3C2–Ni coatings for gears. Surf Eng. 2021;37:80–90.
[28] Peat T, Galloway A, Toumpis A, et al. Performance evaluation of HVOF deposited cermet coatings under dry and slurry erosion. Surf Coat Technol. 2016;300:118–127.
[29] Nieto A, Kimb J, Penkov OV, et al. Elevated temperature wear behavior of thermally sprayed WC-Co/nanodiamond composite coatings. Surf Coat Technol. 2017;315:283–293.
[30] Hong S, Wua Y, Zhang J, et al. Synergistic effect of ultrasonic cavitation erosion and corrosion of WC–CoCr and FeCrSiBMn coatings prepared by HVOF spraying. Ultrason Sonochem. 2016;31:563–569.
[31] Mayrhofer E, Janka L, Mayr WP, et al. Cracking resistance of Cr_3C_2–NiCr and WC–Cr_3C_2–Ni thermally sprayed coatings under tensile bending stress. Surf Coat Technol. 2015;281:169–175.
[32] Sidhu VPS, Goyal K, Goyal R. Hot corrosion behaviour of HVOF-sprayed 93(WC-Cr_3C_2)-7Ni and 83WC-17Co coatings on boiler tube steel in coal fired boiler. Aust J Mech Eng. 2019;17:127–132.
[33] Thawari N, Gullipalli C, Katiyar JK, et al. Influence of buffer layer on surface and tribomechanical properties of laser cladded Stellite 6. Mater Sci Eng B. 2021;263.
[34] Govande AR, Katiyar JK, Sunil BR, et al. Effect of heat treatment environment on the structural characteristics and microhardness of high velocity oxy-fuel sprayed tungsten carbide-cobalt coatings. Mater Sci Eng Technol. 2021;52(12):1346–1354.
[35] Du H, Shin JH, Lee SW. Study on porosity of plasma-sprayed coatings by digital image analysis method. J Therm Spray Technol. 2005;14:453–461.
[36] Berger L-M, Saaro S, Naumann T, et al. Influence of feedstock powder characteristics and spray processes on microstructure and properties of WC–$(W,Cr)_2C$–Ni hardmetal coatings. Surf Coat Technol. 2010;205:1080–1087.
[37] Wang Q, Zhang S, Cheng Y, et al. Wear and corrosion performance of WC-10Co4Cr coatings deposited by different HVOF and HVAF spraying processes. Surf Coat Technol. 2013;218:127–136.
[38] Kim H-C, Shon I-J, Garay JE, et al. Consolidation and properties of binderless sub-micron tungsten carbide

by field-activated sintering. Int J Refract Met Hard Mater. 2004;22:257–264.
[39] Vinayo ME, Kassabji F, Guyonnet J, et al. Plasma sprayed WC–Co coatings: Influence of spray conditions (atmospheric and low pressure plasma spraying) on the crystal structure, porosity, and hardness. J Vac Sci Technol A. 1985;3:2483–2489.
[40] Taimatsu H, Sugiyama S, Kodaira Y. Synthesis of W_2C by reactive hot pressing and its mechanical properties. Mater Trans. 2008;49:1256–1261.
[41] Murthy JKN, Venkataraman B. Abrasive wear behaviour of WC–CoCr and Cr_3C_2–20(NiCr) deposited by HVOF and detonation spray processes. Surf Coat Technol. 2006;200:2642–2652.
[42] Berger L-M, Trache R, Toma F-L, et al. Development of cost-effective hardmetal coating solutions for high-temperature applications, part one: feedstock powders, cost-effectiveness and coating properties. Therm Spray Bull. 2015;8(2):126–136.
[43] DSMTS-0113.7 – WC 10Co 4Cr sintered and crushed powders. Material product data sheet, Oerlikon Metco; 2017. p. 3.
[44] Tarjan I, Debreczeni E. Theoretical and experimental investigation on the wear of pipeline caused by hydraulic transport. In: Coles, NG, Hemmings, SK, editors. Proceedings of the 2nd International Conference on Hydraulic Transport of Solids in Pipes, BHRA, Cranfield, UK; 1972. p. l–14.
[45] Gupta R, Singh SN, Sehadri V. Prediction of uneven wear in a slurry pipeline on the basis of measurements in a pot tester. Wear. 1995;184:169–178.
[46] Elkholy A. Prediction of abrasion wear for slurry pump materials. Wear. 1983;84:39–49.
[47] Gandhi BK, Singh SN, Seshadri V. Study of the parametric dependence of erosion wear for the parallel flow of solid–liquid mixtures. Tribol Int. 1999;32:275–282.
[48] Stachowiak GW, Batchelor AW. Engineering tribology. New York: Elsevier, Amsterdam; 1993, p. 511.
[49] O'Flynn DJ, Bingley MS, Bradley MSA, et al. A model to predict the solid particle erosion rate of metals and its assessment using heat-treated steels. Wear. 2001;248:162–177.
[50] Gee MG, Gee RH, McNaught I. Stepwise erosion as a method for determining the mechanisms of wear in gas borne particulate erosion. Wear. 2003;255:44–54.
[51] Verdon C, Karimi A, Martin JL. Microstructural and analytical study of thermally sprayed WC–Co coatings in connection with their wear resistance. Mater Sci Eng A. 1997;234:731–734.